

Analysis of Stationary-Wave Nonstationarity in the Northern Hemisphere 500-hPa Height Field*

ZHOU Guohua^{1†}(周国华), WANG Panxing¹(王盘兴), SHI Ning¹(施宁), LI Qiaoping²(李巧萍),
and SHE Gaojie¹(佘高杰)

¹ Institute of Atmospheric Sciences, Nanjing University of Information Science & Technology, Nanjing 210044

² National Climate Center, China Meteorological Administration, Beijing 100081

(Received March 30, 2009)

ABSTRACT

In this paper, the concept of stationary-wave nonstationarity is presented and elucidated in the framework of the Lorenz circulation decomposition. This concept indicates the relative magnitude of the zonal non-uniform abnormality to the intensity of stationary waves on the monthly mean scale. Based on the Lorenz circulation decomposition, the nonstationarity degree I_{us} (I_{us}^1) of the global (local) stationary waves is defined, and then used to analyze the stationary-wave nonstationarity at 30°–60°N, where the intensity of stationary waves at 500 hPa in the Northern Hemisphere, as is well known, is very high. The following findings are obtained: (1) There exist seasonal southward and northward movements in the position of the nonstationarity zones of the global stationary waves. The steady stationary waves occur in midlatitudes (35°–55°N) in winter and in the subtropical region (south of 35°N) in summer, associated with the major troughs over East Asia and North America and the weak European trough in winter, and with the relatively steady subtropical high system in summer. A high value center of I_{us} is at 35°N in spring and 50°N in summer, which might be caused by the seasonal variation of stationary-wave intensity, particularly in association with the interannual variability of trough/ridge positions of stationary waves on the monthly mean maps. (2) There exists obvious asymmetry in I_{us}^1 , with the steady zones always located in the areas controlled by strong troughs/ridges and the unsteady ones in the areas where the stationary-wave intensity is low. The I_{us}^1 in the subtropics (south of 35°N) is larger in winter than in summer, and vice versa in the midlatitude region (north of 35°N). The summertime distribution of I_{us}^1 on the whole shows a rather complicated structure. However, North Europe is the most unsteady area for local stationary waves, as represented by high values of I_{us}^1 in both summer and winter, while over the North American continent (about 120°E–60°W), the I_{us}^1 is slightly less than 1 in summer, indicating that the stationary waves in this region are more steady than those over other mid and high latitude regions. (3) From North China to Northwest Pacific, there is a high value zone of I_{us}^1 in summer, with its center (45°N, 130°E) located in the east of Heilongjiang Province. This influences the summer climate of northern China, including Northeast, North, and Northwest China. It is obvious that the nonstationarity is an intrinsic attribute of stationary waves, and can be regarded as being of the same importance as the intensity and energy-spectrum structure of stationary waves in the studies of the general circulation system.

Key words: 500-hPa geopotential height field, stationary waves, nonstationarity, general circulation system

Citation: Zhou Guohua, Wang Panxing, Shi Ning, et al., 2010: Analysis of stationary-wave nonstationarity in the Northern Hemisphere 500-hPa height field. *Acta Meteor. Sinica*, **24**(3), 287–296.

1. Introduction

In the early 1950s, Ye and Zhu (1958) summed up the basic characteristics of geopotential height (\bar{H}) waves in midlatitudes, i.e., being strong in winter and weak in summer with three waves in winter and four waves in summer, based on the 500-hPa climatic charts of \bar{H} in the Northern Hemisphere. Since the 1990s,

Wang and Wu (1995), Li et al. (2000), and Yan and Wang (2006) have analyzed the structure of \bar{H} waves quantitatively with the spherical function method, and verified the existence of the above basic characteristics.

According to the Lorenz (1967) circulation decomposition theory, the waves on the \bar{H} chart are called stationary waves, denoted as \bar{H}^* . As for a specific location and month, \bar{H}^* can be written as \bar{H}^*

*Supported by the National Natural Science Foundation of China under Grant No. 40633018.

†Corresponding author: zgh_qxj@yangzhou.gov.cn.

(Chinese version published in Vol. 67, No. 2, 298–306, 2009)

(λ, ψ, t_m) , where λ is longitude, ψ is latitude, and t_m is the ordinal number of months; \overline{H}^* is constant during the studied time period (e.g., 1958–1997), and can fully determine the two basic characteristics given by Ye and Zhu (1958). Geng and Huang (1996, 1997) proposed “the abnormality of stationary waves,” which refers to the departure of $H^*(t_y)$ in an individual year from the normal \overline{H}^* , where t_y is the ordinal number of years. Meanwhile, they pointed out that in different regions, the anomalous vorticity sources may result in different anomalous stationary waves. Chen and Huang (2005) also demonstrated that there is interannual variation in the anomalous propagation of quasi-stationary planetary waves, and therefore $H^*(t_y)$ varies year by year. It is worthwhile to know in what extent \overline{H}^* can represent $H^*(t_y)$ over the years.

In the framework of the Lorenz circulation decomposition, this paper will focus on the nonstationarity of stationary waves, which indicates the relative magnitude of the climatic variability of zonal component of $H^*(t_y)$ to the intensity of stationary waves on the monthly mean scale. Obviously, the nonstationarity of stationary waves is a new statistical property of the atmospheric general circulation. We explain the nonstationarity of stationary waves through \overline{H}^* and $H^*(t_y)$ at 45°N , and introduce a scheme for quantitatively analyzing the nonstationarity of stationary waves in terms of the Lorenz circulation decomposition. The key part in the scheme is that the nonstationarity of

stationary waves (I_{us}) is defined, as a measure of the non-stationary degree of stationary waves. In addition, the geographic distribution and seasonal variation of the nonstationarity of the global/local stationary waves within $30^\circ\text{--}60^\circ\text{N}$ are analyzed, and the relation with the stationarity of climate in winter and the abnormality of climate in summer are discussed.

2. Concept of the stationary-wave nonstationarity

Figure 1 shows distributions of \overline{H} along 45°N at 500 hPa in January and July of 1958–1997. It can be seen that the stationary waves are stronger in January than those in July: there is a clear pattern of “3 troughs and 3 ridges” in January with the trough along the Ural Mountains (60°E) obviously weaker than the troughs around East Asia (147.5°E) and North America (287.5°E); in July the pattern of “4 troughs and 4 ridges” becomes less typical due to the frequent small fluctuations over the northeastern Asia and northern Pacific.

The analysis of the harmonic-wave variance contribution of the zonal component of \overline{H}^* along 45°N to the total geopotential height field shows that the variance contributions of “wave 1” in January and July are the greatest, accounting for about 50%; the variance contributions of “waves 3” in January and “waves 4” in July are the second greatest. This is consistent with

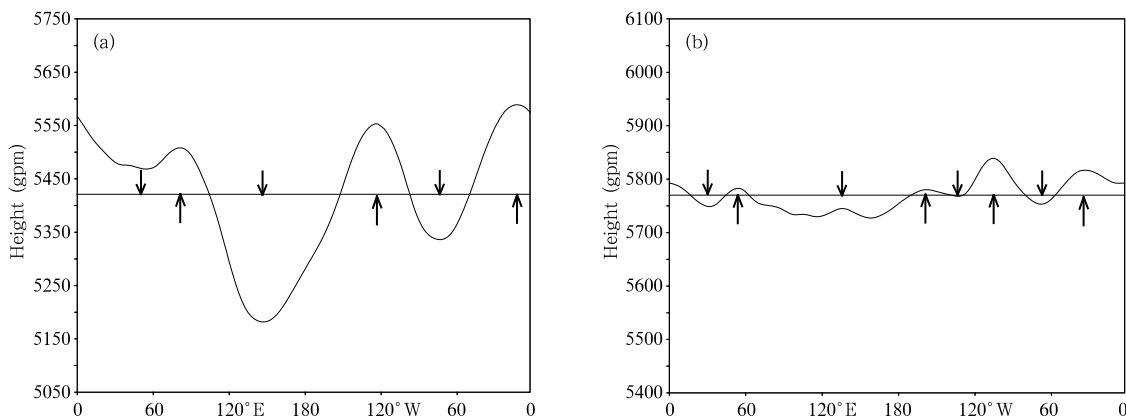


Fig. 1. Distributions of the 40-yr (1958–1997) mean geopotential height \overline{H} along 45°N at 500 hPa in (a) January and (b) July. Symbols \uparrow and \downarrow denote locations of ridges and troughs, respectively. Straight lines denote the zonal averages of geopotential height $[\overline{H}]$ along 45°N , which are 5421 and 5770 gpm in January and July, respectively.

the characteristics of stationary waves, i.e., “3 waves in winter and 4 waves in summer”. In addition, the variance contributions of “wave 2” in January and especially “waves 5 and 6” in July are also great, being close to those of “wave 4” and “wave 3” in January and

July. Therefore, the wave power in the wavenumber domain of the 500-hPa mean height in midlatitudes is dominated by 4 to 6 waves (long waves) in July but by 2 to 3 waves (ultra-long waves) in January.

Table 1. Variance contributions (%) of the zonal harmonic-wave components of \overline{H}^* along 45°N

Wave number	1	2	3	4	5	6	7	8	9	10
January	44.7	23.8	27.9	2.5	1.0	0.1	0.0	0.0	0.0	0.0
July	59.1	4.4	4.1	10.3	10.1	7.2	2.8	0.3	1.2	0.0

Figure 2 displays $\{H^*(t_y), t_y = 1, \dots, 40\}$, the aggregation of waves in the 500-hPa height field along 45°N during 1958–1997 in January and July, abbreviated as $H^*(t_y)$ and defined by Eq. (2) below. It can be seen that the numbers, positions, and intensities of troughs and ridges of $H^*(t_y)$ in January are generally close to those of the stationary waves of the corresponding \overline{H}^* (Fig. 1). However, the discrepancies between them vary with longitudes. According to the natural climatic region division (Zhang, 1959), in January, the $H^*(t_y)$ and \overline{H}^* are very close over the Asian region (60°E to 165°W) and North America (165° to 45°W) for most years, but greatly different in the European region (45°W to 105°E); in July, they are much different, except for some areas in North America (135° to 45°W) and Europe (15° to 60°E). The differences between $H^*(t_y)$ and \overline{H}^* along 45°N indicate that as a mean attribute of individual zonal waves $H^*(t_y)$ for multiple years, the climatological stationary waves (\overline{H}^*) also vary with season and geographical location.

The concept of the stationary-wave nonstationarity is used to illustrate the relative difference between the annual mean zonal waves $H^*(t_y)$ and the climatological stationary waves \overline{H}^* . From the above analysis, we conclude that the stationary waves are nonstationary over the regions/seasons where/when small-amplitude \overline{H}^* and big differences between $H^*(t_y)$ and \overline{H}^* in wave number, phase, and amplitude (Fig. 2) coexist; otherwise they are stationary. Obviously, the nonstationarity of stationary waves is a new statistical property of the atmospheric general circulation, and it describes an attribute other than the intensity and trough/ridge numbers of stationary waves.

3. Calculation of the nonstationarity of stationary waves

The stationary-wave nonstationarity is a measure of the non-stationary degree of stationary waves. Li et al. (2003) defined the nonstationarity of spherical stationary waves (two-dimensional) in the height field

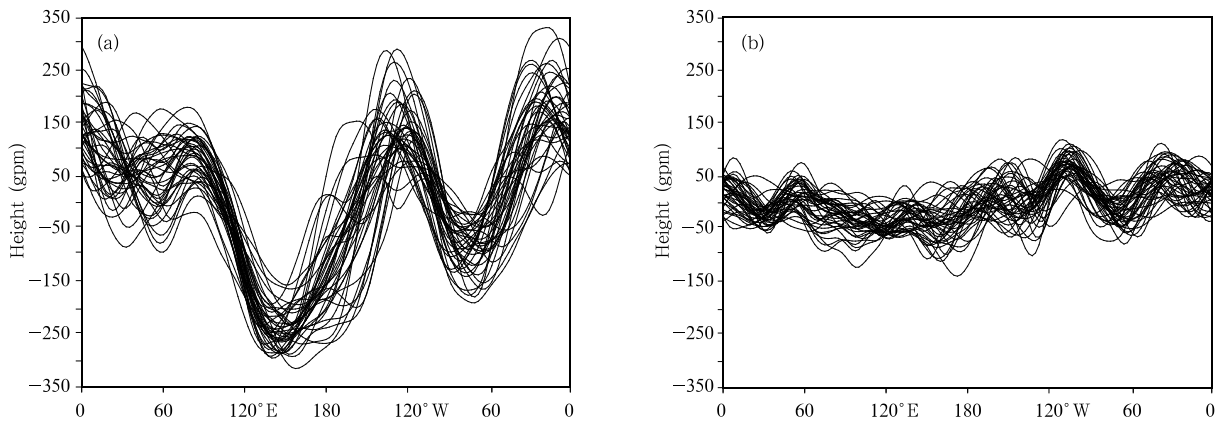


Fig. 2. Latitudinal distributions of $H^*(t_y)$ (zonal components of geopotential height at 500 hPa) along 45°N in (a) January and (b) July from 1958 to 1997.

over the Northern and Southern Hemisphere, and obtained a series of meaningful findings about the spatial-temporal characteristics of the height field. In this paper, we analyze the nonstationarity of stationary waves along a certain latitude (one dimensional) based on the Lorenz circulation decomposition.

The NCEP/NCAR monthly 500-hPa height $H(i, j, t_m, t_y)$ data in the Northern Hemisphere from 1958 to 1997 are used, with a grid spacing of 2.5° . The relations between grid ordinal numbers i and j , and longitude λ_i and latitude φ_j are given as follows: $\lambda_i = i\Delta\lambda$, $\varphi_j = j\Delta\varphi$, where $i = 0, \dots, 143$, $j = 0, \dots, 36$. t_m and t_y are the ordinal numbers of month and year with the range of $t_m = 1-12$, and $t_y = 1-40$. The decomposition equation in time domain is given by

$$H(i, j, t_m, t_y) = \overline{H}(i, j, t_m) + H'(i, j, t_m, t_y), \quad (1)$$

and the decomposition equation in space domain $\lambda \in [0, 360^\circ)$ is given by

$$H(i, j, t_m, t_y) = [H](j, t_m, t_y) + H^*(i, j, t_m, t_y), \quad (2)$$

where “ $\overline{\quad}$ ” is the normal arithmetic mean over 40 yr; “[\quad]” denotes the arithmetic mean along a latitudinal circle; “ $'$ ” denotes anomaly relative to the climatological mean, and “ $*$ ” is the latitude partial-differential operator, i. e., deviation from the latitudinal mean.

The spatial domain decomposition is conducted on the first term of the right side of Eq. (1):

$$\overline{H}(i, j, t_m) = [\overline{H}](j, t_m) + \overline{H}^*(i, j, t_m), \quad (3)$$

where $[\overline{H}](j, t_m)$ is the zonal mean of \overline{H} at φ_j and t_m on the climatological map, independent of stationary waves; $\overline{H}^*(i, j, t_m)$ denotes stationary waves in t_m at λ_i and φ_j , which can also be obtained from the time mean of the second term of the right side of Eq. (2). In Fig. 1, the curve denotes \overline{H} along 45°N ($i = 0, \dots, 143$; $j = 18$) with t_m being January and July, and the straight line is for $[\overline{H}]$.

The anomaly can also be decomposed into

$$H'(i, j, t_m, t_y) = [H'](j, t_m, t_y) + H'^*(i, j, t_m, t_y), \quad (4)$$

where $[H'](j, t_m, t_y)$ is the mean anomaly along a latitudinal cycle (i.e., zonal uniformity). It is independent

of the wave abnormality in year t_y at φ_j , but related to the abnormality of zonal mean height at 500 hPa and the abnormality of zonal mean air temperature below 500 hPa. The second term of the right side of Eq. (4) is the wave abnormality in t_m at φ_j (i.e., zonal non-uniformity), which is the deviation of the waves in t_y at φ_j from stationary waves.

According to Eqs. (3) and (4), the following parameters are defined:

(1) Intensity of stationary waves

$$I_c(j, t_m) = \left\{ \sum_{i=0}^{143} \overline{H}^{*2}(i, j, t_m)/144 \right\}^{1/2}, \quad (5)$$

which is the measure of the strength of stationary waves in t_m at φ_j .

(2) Intensity of zonal non-uniform abnormality in t_y :

$$a(j, t_m, t_y) = \left\{ \sum_{i=0}^{143} H'^*(i, j, t_m, t_y)/144 \right\}^{1/2}, \quad (6)$$

which is the intensity of wave abnormality in t_y and t_m at φ_j .

(3) Intensity of climatological zonal non-uniform abnormality:

$$\begin{aligned} I_a(j, t_m) &= \left\{ \sum_{t_y=1}^{40} \left(\sum_{i=0}^{143} H'^*(i, j, t_m, t_y)/144 \right) / 40 \right\}^{1/2} \\ &= \left\{ \sum_{t_y=1}^{40} a^2(j, t_m, t_y) / 40 \right\}^{1/2}, \end{aligned} \quad (7)$$

which is the climatic variability of wave intensity in t_m at φ_j .

(4) Nonstationarity degree of stationary waves:

$$I_{us}(j, t_m) = I_a(j, t_m) / I_c(j, t_m), \quad (8)$$

which is the ratio of the climatological zonal non-uniform abnormality to the stationary wave intensity in t_m at φ_j .

4. Analysis of I_{us}

Based on the analysis of the variation of stationary-wave intensities (I_c) for various months, we focus on the latitudinal zone with greater I_c over the

whole year and study the variation of I_{us} for the stationary waves with season (t_m) and latitude (φ) in the global domain, then give the definitions of the intensities and nonstationarity degree of the local stationary waves (I_c^1 and I_{us}^1) and analyze their variation with season (t_m) and geographical location (λ, φ). The global domain refers to $\lambda \in [0, 360^\circ]$.

4.1 Seasonal variation of the global-domain stationary-wave intensity (I_c)

Figure 3 shows the calculation results of $I_c(j, t_m)$. It can be seen that the stationary-wave intensity is greater within 30° – 75°N , higher in winter and lower in summer; the strongest stationary waves show up around 50°N except in July and August, when there are two maximum values of I_c appearing around 62.5°N (main) and 40°N (minor). Based on the experiences in analyzing the climate abnormality in China, the region of 30° – 60°N ($j = 12$ – 24) is selected as the key latitudinal zone for the study of stationary-wave nonstationarity.

4.2 Variations of I_{us}

From the latitude-time cross-sections of the global-domain I_{us}, I_a , and I_c within 30° – 60°N (Fig. 4), the following conclusions are obtained. (1) The largest I_{us} zone of stationary waves (indicated by the thick line in Fig. 4a) shows an obvious annual variation. It moves northward from 30°N in March and April, reaches the farthest north position in July and August, and comes back to 30°N in November and December. During this period, the speed of the northward/southward movement and the I_{us} values alter,

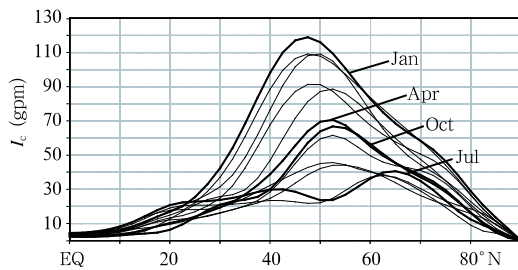


Fig. 3. Longitudinal variations of I_c (stationary-wave intensity) in different months for the 500-hPa \overline{H} field. The thick lines denote I_c in January, April, July, and October, respectively.

with a quicker northward movement and smaller nonstationary degree ($I_{\text{us}} < 1$) in June. This can be the reflection of the “sudden change of the atmospheric circulation in June” (Ye et al., 1958) in the nonstationarity of stationary waves. (2) The stationarity of stationary waves is the greatest in midlatitudes in winter and in the subtropical region in summer. This is mainly attributed to the stronger stationary waves (Fig. 4b) in winter and to both weaker climatological zonal non-uniform intensity (Fig. 4c) and the higher stationary-wave intensity (Fig. 4b) in summer. (3) The nonstationarity of the stationary waves is the greatest in the subtropical region in winter and in midlatitudes (around 50°N) in summer. This is mainly determined by both the weaker stationary waves (Fig. 4b) in winter and the stronger climatological zonal non-uniform intensity (Fig. 4c) in summer.

5. Analysis of I_{us}^1

It is found out through analyzing Figs. 1 and 2 that the deviations of $H^*(t_y)$ from \overline{H}^* vary in different longitudes for a specific month. Therefore, it is necessary to examine the non-stationary degrees of stationary waves in local domains (I_{us}^1) and their zonal variations (only in January and July between 30° – 60°N).

5.1 Definition of I_{us}^1

At latitude φ_j , a domain (D) centered around λ_i is selected, with the width being $2i_0\Delta\lambda$ from λ_{i-i_0} to λ_{i+i_0} , consisting of $(2i_0 + 1)$ grid points. The zonal mean operator for a local domain is defined as:

$$[f]^1(i) = \left\{ \begin{array}{l} \sum_{i'=i-(i_0-1)}^{i+(i_0-1)} f(i') \\ + \frac{1}{2} [f(i-i_0) + f(i+i_0)] \end{array} \right\} / (2i_0). \quad (9)$$

Using operator $[]^1$ to replace $[]$ in Eqs. (2)–(8), we obtain the definition equations for the intensity of a local stationary wave (I_c^1), the intensity of the local climatological zonal non-uniform abnormality (I_a^1), and the nonstationarity of the local stationary wave (I_{us}^1).

5.2 Variations of I_{us}^1

Based on the feature of “3 waves in winter” and

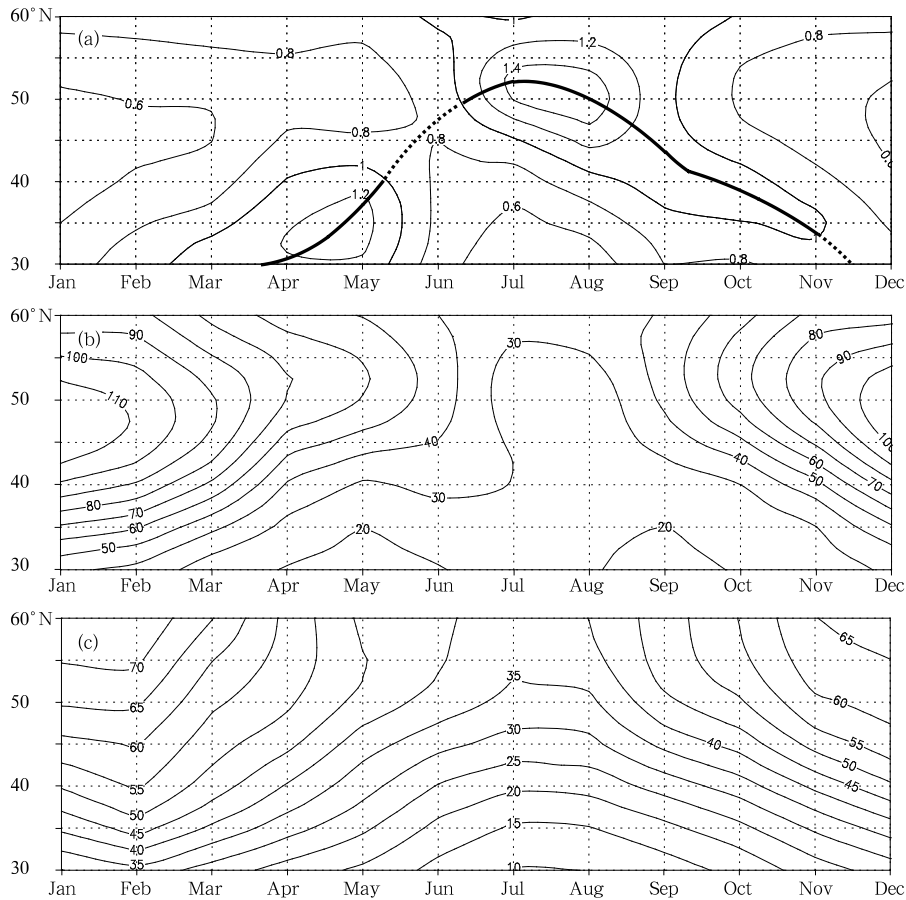


Fig. 4. Latitude-time (month) evolution of (a) I_{us} , (b) I_c , and (c) I_a . The thick line denotes the most non-stationary zone of stationary waves with the part of $I_{us} < 1$ dashed.

“4 waves in summer,” we set λ_i of the domain D to be 120°E and 90°E for January and July (the corresponding j_0 is 24 and 18) respectively, and the distributions of I_c^1 , I_a^1 , and I_{us}^1 between 30° and 60°N are obtained (Figs. 5, 6).

In January, over the most part of the domain, $I_{us}^1 < 1$, but the whole European continent is controlled by high nonstationarity ($I_{us}^1 \geq 1.6$) with the center around Russia (55°N , 32.5°E). It is induced by both the weak European trough (Fig. 5b) and the strong wave abnormality (Fig. 5c). The mid and high latitudes of Asia and the Pacific are the most stationary (having a large area of $I_{us}^1 < 0.6$), with the center over Mongolia and the southeastern Aleutian Islands. This is behind the strong and stationary East Asian trough and the West American ridge.

In July, in most part of the region, $I_{us}^1 > 1$, the nonstationarity of local stationary waves obviously in-

creases. The zone of high nonstationarity ($I_{us}^1 > 2.0$) extends southeastward from North Europe to East Asia, and can be divided into two systems: one is centered around North Europe, distributed zonally, with the center lying slightly southwestward; the other is the strong nonstationarity belt extending northeastward from the North China Plain to the southern Aleutian Islands with the center in the eastern Heilongjiang Province (45°N , 130°E). The two systems are mainly resulted from the drastic decrease of the regional summer stationary-wave intensity. Li and Ji (2001) held that the regions having persistent abnormality in summer in the Northern Hemisphere include a) the region from North Pacific to West Pacific and b) the area from North Atlantic to the west coast of Europe. The geographical locations of the summer nonstationary zones derived in this paper are in agreement with the previous result.

6. Causes and significance of the stationary-wave nonstationarity

The nonstationarity degree of stationary waves I_{us} (I_{us}^1) defined in this paper consists of the intensity of zonal non-uniform abnormality I_a (I_a^1) and the intensity of stationary waves I_c (I_c^1) (Eq. (8)). In the region where the intensity of stationary-wave abnormality is large, and the intensity of stationary waves is small, greater I_{us} (I_{us}^1) can be seen.

Figure 4a shows the latitude-time evolution of I_{us} . In spring, a) the winter stationary waves (mainly East Asian trough, North American trough, and European trough) within 30° – 40° N weaken obviously; b) the summer stationary waves (mainly subtropical high (Liu and Wu, 2000) and continent low) have not yet reached this latitude zone; c) the intensity of stationary waves reaches its minimum (Fig. 4b), and d) the

intensity of zonal non-uniform abnormality remains relatively large (Fig. 4c), so there appears a maximum I_{us} within 30° – 40° N. In summer (July–August), the I_c at 50° N reaches a minimum while the I_a shows only a minor decrease, so I_{us} obtains a maximum at this latitude. In fall, there appears a process reverse to that in spring in the region to the south of 50° N, leading to a maximum I_{us} in this region. Therefore, the extremely large I_{us} zone is mainly attributed to the weakening of stationary waves during the seasonal transition of the atmosphere. The latter is often considered a result of the seasonal variation of stationary waves in the mid-latitude temperature field of the lower troposphere.

The horizontal distributions of I_{us}^1 (Figs. 5a, 6a) reveal more clearly the zonal difference in January and July. From January to July, there always exists an area with a greater I_{us}^1 in the northern Europe. It is known from the climatological wave chart (figure omit-

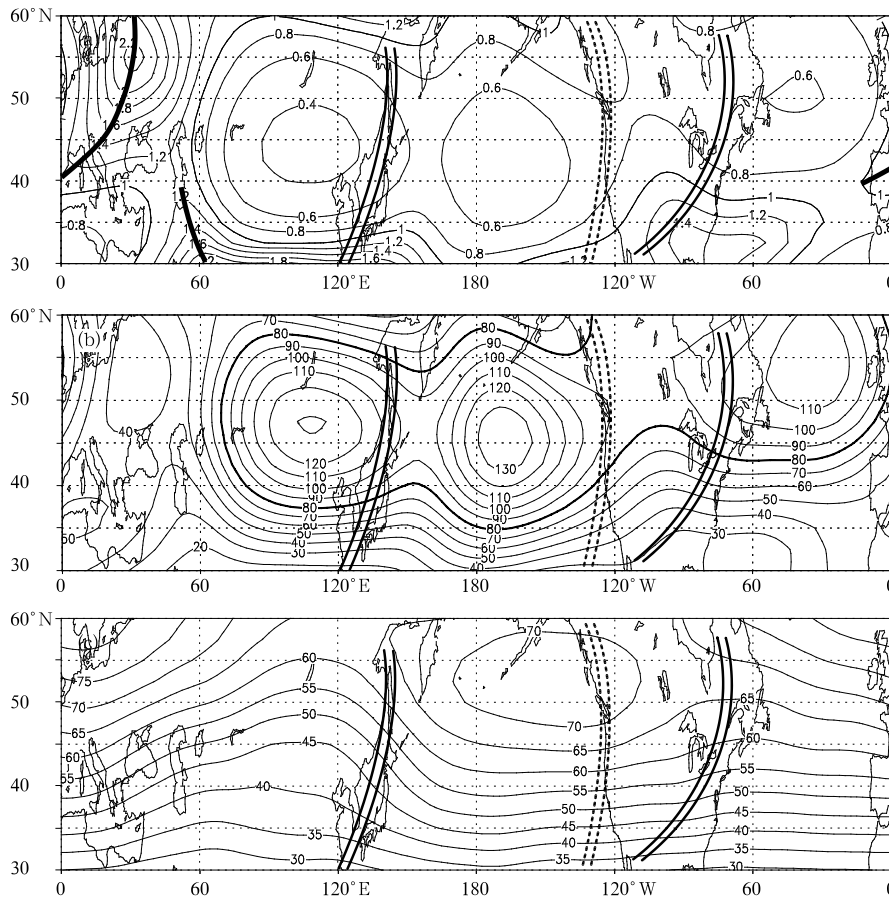


Fig. 5. Distributions of local stationary-wave statistics in January of (a) I_{us}^1 , (b) I_c^1 , and (c) I_a^1 . The double solid (dashed) lines denote the trough (ridge) lines of stationary waves, and the thick solid lines delineate the zone of high nonstationarity.

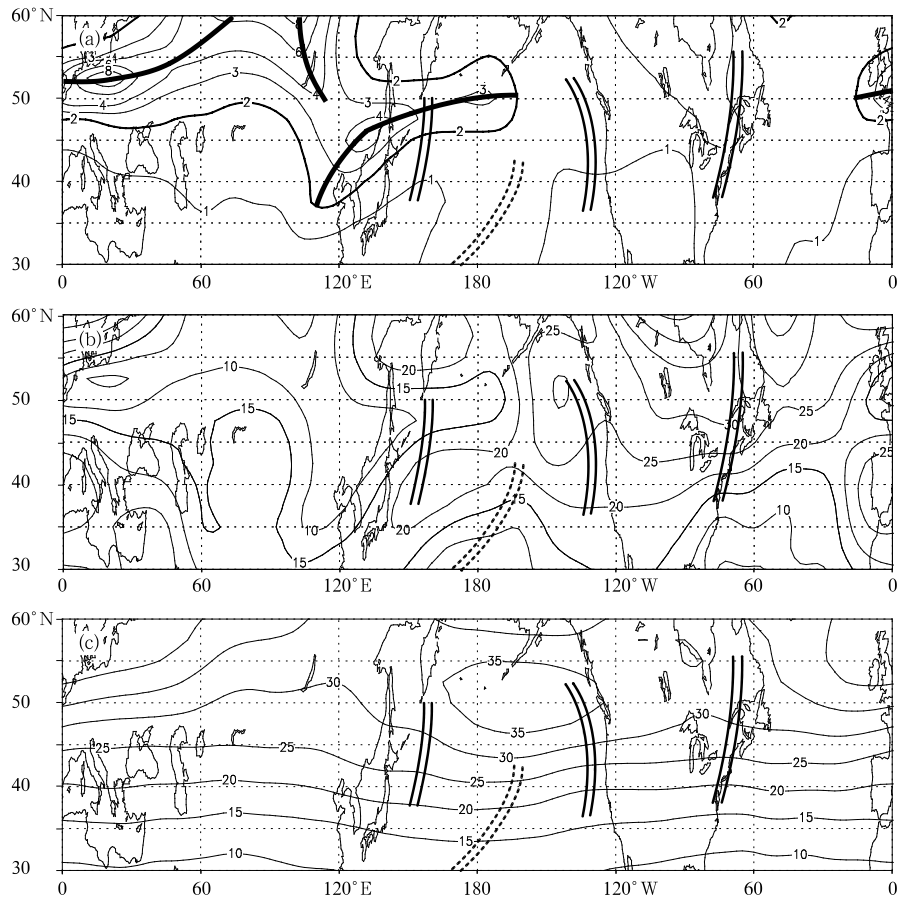


Fig. 6. As in Fig. 5, but for July.

ted) that waves in this area are relatively weak, and I_c^1 is smaller. Meanwhile, since the area is located around the exit of the Atlantic jet, where disturbances occur frequently and the trough/ridge distribution in the area changes easily, resulting in the frequent interannual variation of circulation patterns in the area; that is, I_a^1 is greater. The greater I_a^1 and smaller I_c^1 eventually lead to the occurrence of maximum I_{us}^1 . From winter to summer, there appears a new non-stationary zone with the center around the eastern Heilongjiang Province, where the greater I_{us}^1 is closely related to the smaller I_c^1 (Fig. 6b). The East Asian trough moves from the East Asian coast to the vicinity of the Kamchatka Peninsula from spring to summer. The circulation pattern in the area from Northeast China to the central Pacific becomes obviously straight and smooth. Especially, since the area around Northeast China is controlled by a weak ridge behind the East Asian trough, a low I_c^1 center ($I_c^1 < 10$) appears over

there. Similarly, the maximum I_{us}^1 in the tropical region showing up only in winter (January) is mainly caused by the minimum I_c^1 .

It should be pointed out that the maximum non-stationarity zone from North China, through Northeast China, to North Pacific (south of 50°N) is the only nonstationarity zone of the stationary waves in summer. From the definition of I_{us}^1 , we find that this area, extending east and westward with a span of 90 longitude degrees (including East, North, and Northwest China), has the largest interannual variation in the summer mean circulation waves, compared with other areas at the same latitudes. Considering the carbon cycle (Rayner et al., 1999), a vast area of Northeast China is in the balance of carbon budget (source/sink). This indicates, from another viewpoint, that the carbon balance in this area is vulnerable and can be easily affected by the climate change. The climate change may turn this area from being in carbon

balance into a carbon source. In recent years, some Chinese researchers (Fu and Ye, 1995; Fu et al., 2003; Lian et al., 2005) pointed out that in some specific geographical regions, the interannual variability of the climate, environment and ecological system is strong and complicated, thus these regions are called sensitive or vulnerable regions. The Intergovernmental Panel on Climate Change (IPCC) has defined a concept of vulnerability of the society to climate change (IPCC, 2001). Lian et al. (2005) found that Northeast China, Inner Mongolia (North China), and Northwest China are the typical sensitive and vulnerable regions ecologically. These are basically in agreement with the areas of high stationary-wave nonstationarity described in this paper. Our results reveal that Northeast China, North China, Northwest China, Mongolia, and Russian Far East, are the areas with strong stationary-wave nonstationarity at 500 hPa in summer, which could be the dynamical cause of the climate vulnerability in these areas. The corresponding local areas in North America (about 120°–160°W), with I_{us}^1 slightly less than 1, are the areas with relatively steady stationary waves in summer. Therefore, the mid and high latitudes of the North American continent exhibit the least climate abnormality in summer.

In summary, the nonstationarity of stationary waves is an intrinsic statistical attribute of stationary waves. It should be of the same significance as the intensity and energy-spectral structure of stationary waves of the atmosphere.

7. Conclusions

In this paper, the concept of stationary-wave nonstationarity is presented and elucidated in the framework of the Lorenz circulation decomposition. The stationary-wave nonstationarity indicates the relative magnitude of the zonal non-uniform abnormality to the intensity of stationary waves on the monthly mean scale. Based on the Lorenz circulation decomposition, the nonstationarity degree I_{us} (I_{us}^1) of the global (local) stationary waves is defined, and then used to analyze the stationary-wave insatiability between 30° and 60°N, where the intensity of stationary waves in the Northern Hemisphere 500-hPa geopoten-

tial height, as is well known, is significantly high. The following conclusions are obtained:

(1) There exist seasonal southward and northward movements in the position of I_{us} zones of the global stationary waves. The non-stationary height center appears at 35°N in spring and 50°N in summer; the stationary zone appears in midlatitudes (35°–55°N) in winter and in the subtropical region (south of 35°N) in summer.

(2) The nonstationarity of local stationary waves is greater in winter than in summer in the subtropical region (south of 35°N), and vice versa in midlatitudes (north of 35°N). The summer geographical distribution of I_{us}^1 displays a rather complicated structure.

(3) From North China to Northwest Pacific, there is a high value zone of I_{us}^1 in summer, with its center (45°N, 130°E) located to the east of Heilongjiang Province. It influences the northern China, including Northeast, North, and Northwest China, and can explain why these areas become vulnerable climatically in summer.

(4) It is obvious that the nonstationarity is an intrinsic attribute of stationary waves, and it can be regarded as of the same importance as the intensity and energy-spectrum structure of stationary waves in the studies of the atmospheric general circulation.

Acknowledgements. Special thanks to Profs. Ji Liren and Bueh Cholaw of the Institute of Atmospheric Physics, Chinese Academy of Sciences for their valuable comments and suggestions, and the Nanjing Atmospheric Data Service Center of the Department of Earth Sciences of National Science Foundation of China (NSFC) for their help in data collection.

REFERENCES

- Chen Wen and Huang Ronghui, 2005: The three-dimensional propagation of quasi-stationary planetary waves in the Northern Hemisphere winter and its interannual variations. *Chinese J. Atmos. Sci.*, **29**(1), 137–146. (in Chinese)
- Fu Congbin and Ye Duzhen, 1995: Global change and the future trend of ecological environment evolution in China. *Scientia Atmos. Sinica*, **19**(1), 116–126. (in Chinese)

- , Dong Wenjie, Wen Gang, et al., 2003: Regional response and adaptation to global change. *Acta Meteor. Sinica*, **61**(2), 245–250. (in Chinese)
- Geng Quanzhen and Huang Ronghui, 1996: The forcing of anomalous divergent wind and transient vorticity fluxes to the anomaly of stationary waves. *Acta Meteor. Sinica*, **54**(2), 132–141. (in Chinese)
- and —, 1997: Maintenance mechanisms of upper tropospheric stationary wave anomaly teleconnection patterns. *Acta Meteor. Sinica*, **55**(1), 22–32. (in Chinese)
- IPCC, 2001: Climate Change 2001. Impacts, Adaptation and Vulnerability. Contribution of Working Group II to the Third Assessment Report of the Intergovernmental Panel on Climate Change. McCarthy J. J., Canziani O. F., Leary N. A., et al., eds. Cambridge University Press, United Kingdom, 1032 pp.
- Li Qiaoping, Wang Panxing, and Li Liping, 2003: Some circulation indices and their variation character of hemispherical monthly mean geopotential height fields. *J. Nanjing Institute Meteor.*, **26**(3), 341–348.
- Li Shuanglin and Ji Liren, 2001: Persistent anomaly in Ural area in summer and its background circulation characteristics. *Acta Meteor. Sinica*, **59**(3), 280–293. (in Chinese)
- Li Yafen, Wang Panxing, Zhang Ruigui, et al., 2000: Analysis on the spatial/temporal structure of global atmospheric climatic geopotential height fields. *J. Nanjing Institute Meteor.*, **23**(4), 494–504.
- Lian Yi, Shen Bozhu, Gao Zongting, et al., 2005: Correlation of drought development tendency in China's climate transition zone and activity of East Asian summer monsoon and polar vortex. *Acta Meteor. Sinica*, **63**(5), 740–749. (in Chinese)
- Liu Yimin and Wu Guoxiong, 2000: Reviews on the study of the subtropical anticyclone and new insights on some fundamental problems. *Acta Meteor. Sinica*, **58**(4), 500–512. (in Chinese)
- Lorenz, E. N., 1967: *The Nature and Theory of the General Circulation of the Atmosphere*. World Meteorological Organization. (in Chinese)
- Rayner, P. J., I. G. Enting, R. J. Francey, et al., 1999: Reconstructing the recent carbon cycle from atmospheric CO₂, delta 13 C and O₂/N₂ observations. *Tellus*, **51**(B), 213–232.
- Wang Panxing and Wu Hongbao, 1995: Analysis of spherical function spectral structure of northern 500-hPa monthly mean height. *Acta Meteor. Sinica*, **9**(2), 237–248.
- Yan Jusheng and Wang Panxing, 2006: Spherical function analysis of the climatic change rate of globally atmospheric geopotential height fields. *J. Appl. Meteor. Sci.*, **17**(2), 145–150. (in Chinese)
- Ye Duzheng, Tao Shiyan, and Li Maicun, 1958: The abrupt change of circulation over Northern Hemisphere during June and October. *Acta Meteor. Sinica*, **29**(4), 249–263. (in Chinese)
- Ye Duzheng and Zhu Baozhen, 1958: *Several Fundamental Problems in the General Circulation of the Atmosphere*. Science Press, Beijing, 158 pp.
- Zhang Jijia, 1959: Development in the synoptic methods of Murtanovski school long-range weather prediction in USSR. *Acta Meteor. Sinica*, **30**(4), 376–389. (in Chinese)